



High-resolution Spectroscopy of the GD-1 Stellar Stream Localizes the Perturber near the Orbital Plane of Sagittarius

Ana Bonaca¹ , Charlie Conroy¹ , David W. Hogg^{2,3,4,5} , Phillip A. Cargile¹ , Nelson Caldwell¹ , Rohan P. Naidu¹ ,
Adrian M. Price-Whelan⁵ , Joshua S. Speagle¹ , and Benjamin D. Johnson¹

¹ Center for Astrophysics|Harvard & Smithsonian, 60 Garden Street, Cambridge, MA 02138, USA; ana.bonaca@cfa.harvard.edu

² Center for Cosmology and Particle Physics, Department of Physics, New York University, USA

³ Center for Data Science, New York University, USA

⁴ Max-Planck-Institut für Astronomie, Heidelberg, Germany

⁵ Center for Computational Astrophysics, Flatiron Institute, 162 Fifth Avenue, New York, NY 10010, USA

Received 2020 January 16; revised 2020 March 10; accepted 2020 March 14; published 2020 April 6

Abstract

The 100° long thin stellar stream in the Milky Way halo, GD-1, has an ensemble of features that may be due to dynamical interactions. Using high-resolution MMT/Hectochelle spectroscopy we show that a spur of GD-1-like stars outside of the main stream are kinematically and chemically consistent with the main stream. In the spur, as in the main stream, GD-1 has a low intrinsic radial velocity dispersion, $\sigma_{v_r} \lesssim 1 \text{ km s}^{-1}$, is metal-poor, $[\text{Fe}/\text{H}] \approx -2.3$, and has little intrinsic spread in the $[\text{Fe}/\text{H}]$ and $[\alpha/\text{Fe}]$ abundances, which point to a common globular cluster progenitor. At a fixed location along the stream, the median radial velocity offset between the spur and the main stream is smaller than 0.5 km s^{-1} , comparable to the measurement uncertainty. A flyby of a massive, compact object can change orbits of stars in a stellar stream and produce features like the spur observed in GD-1. In this scenario, the radial velocity of the GD-1 spur relative to the stream constrains the orbit of the perturber and its current on-sky position to $\approx 5000 \text{ deg}^2$. The family of acceptable perturber orbits overlaps the stellar and dark-matter debris of the Sagittarius dwarf galaxy in present-day position and velocity. This suggests that GD-1 may have been perturbed by a globular cluster or an extremely compact dark-matter subhalo formerly associated with Sagittarius.

Unified Astronomy Thesaurus concepts: Tidal tails (1701); High resolution spectroscopy (2096); Milky Way dynamics (1051); Milky Way dark matter halo (1049)

1. Introduction

The pre-eminent cosmological model predicts that galaxies like the Milky Way contain a myriad of non-luminous clumps of dark matter (e.g., Diemand et al. 2008; Springel et al. 2008). Masses of these dark-matter subhalos are $\gtrsim 4$ orders of magnitude lower than the total mass of the Milky Way, so they are expected to have a negligible effect on most stars in the Galaxy (e.g., Hopkins et al. 2008; D’Onghia et al. 2010). However, even low-mass subhalos would leave evidence of interaction with stellar streams, the tidal debris of luminous satellites. Numerical experiments have shown that subhalo encounters can heat up streams (e.g., Ibata et al. 2002; Johnston et al. 2002), produce gaps in their density profiles (e.g., Siegal-Gaskins & Valluri 2008; Yoon et al. 2011), and cause stream folds (e.g., Carlberg 2009).

Until recently, observations of stellar streams in the Milky Way were insufficient to allow robust searches for signatures of dark-matter subhalos (see Carlberg et al. 2012; Ibata et al. 2016). Now, proper motions from the Gaia mission (Gaia Collaboration et al. 2018) have revolutionized our ability to discover (e.g., Malhan et al. 2018; Meingast et al. 2019) and characterize stellar streams (e.g., Bonaca et al. 2019a; Shipp et al. 2019). Using Gaia data, Price-Whelan & Bonaca (2018) studied the nearby, retrograde stellar stream GD-1 (Grillmair & Dionatos 2006), produced the cleanest map of a stream in the Milky Way and identified several underdensities with high confidence, as well as stars outside of the main stream (see also de Boer et al. 2019; Malhan et al. 2019b). Bonaca et al. (2019b) created dynamical models of GD-1 that, following an encounter with a massive object, form a stream gap and an

adjacent spur of stars that quantitatively match the observed features. With no known luminous object having approached GD-1 sufficiently close, there is a possibility that GD-1 was perturbed by a dark-matter subhalo.

Precise kinematic data are required to test whether the spur-and-gap feature in GD-1 was indeed formed in an interaction with a massive, dark object (Bonaca et al. 2019b). Until now, radial velocities have only been available in the main GD-1 stream and at low precision (Koposov et al. 2010; Huang et al. 2019). In Section 2 we present the high-resolution spectroscopy from MMT/Hectochelle, which we used to define a sample of highly probable GD-1 members in the main stream and in the spur (Section 3). These data show that the spur is kinematically associated with the GD-1 stream (Section 4). The small relative velocity between the stream and the spur can be explained within the impact scenario, but only if a perturber is on a specific set of orbits (Section 5), which improves prospects of locating dark objects within the Milky Way purely from their interactions with stellar streams.

2. Spectroscopy

We observed the GD-1 stellar stream using the MMT/Hectochelle multi-object spectrograph (Szentgyorgyi et al. 2011). Focusing on the perturbed area at $\phi_1 \approx -40^\circ$ ($\phi_{1,2}$ are coordinates oriented along and perpendicular to GD-1, respectively; Koposov et al. 2010), we targeted four fields in the main stream, and four fields in the lower-density spur (Figure 2, top). From a cross-match of the Gaia Data Release 2 (DR2) catalog (Gaia Collaboration et al. 2018) with the *Pan-STARRS* photometric catalog (Chambers et al. 2016), we

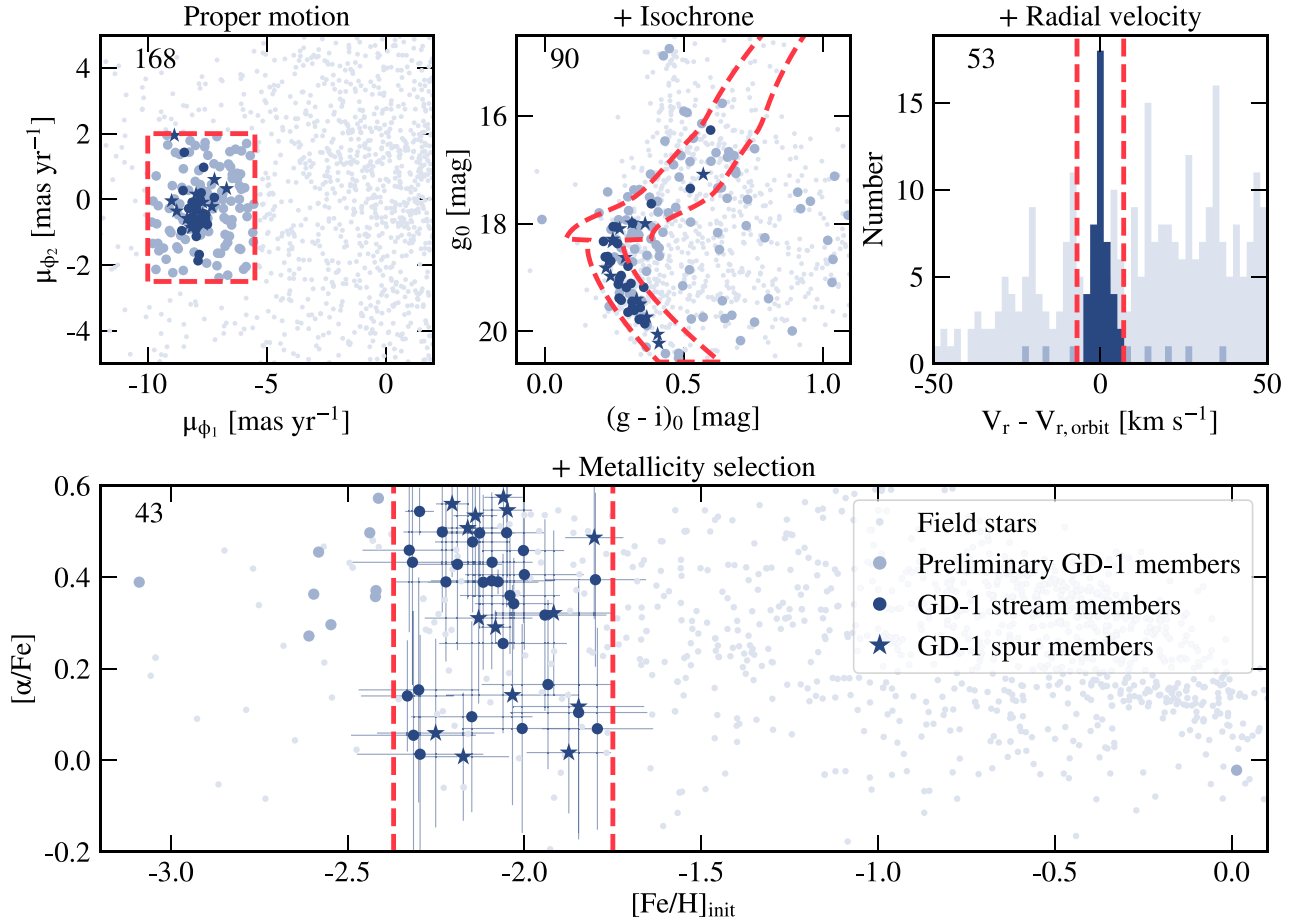


Figure 1. We defined membership to the GD-1 stream with four selection criteria: (1) proper motion box (top-left panel), (2) isochrone box (top-middle panel), (3) small radial velocity offset from the GD-1 orbit (top-right panel), (4) low metallicity (bottom panel). Starting clockwise with the proper motion selection, panels add selections marked with pink dashed lines and decrease membership to the number in the top right of the panel. In each panel, the non-members, preliminary, and high-probability members are shown in light, medium, and dark blue, respectively. The GD-1 spur (stars) is kinematically and chemically consistent with the main stream (circles).

selected retrograde stars as science targets, first prioritizing stars on the GD-1 main sequence, and then its red giant branch (see Price-Whelan & Bonaca 2018). On average, we dedicated $\gtrsim 170$ fibers to science targets per field, for a total of 1409 science spectra. Up to 40 of the remaining fibers were used to estimate the sky emission. We used the RV31 filter covering the Mg b triplet and observed each field for 2.25 hr (except for the stream field at $\phi_1 \approx -34^\circ$, which was observed for 2 hr due to scheduling constraints). With 2×3 spatial and spectral binning of the charge-coupled device (CCD) pixels, we achieved a signal-to-noise ratio (S/N) ≈ 2 at $g = 20$ and an effective resolution $R \approx 32,000$.

The 2D spectra were reduced by *HSRED* v2.1.⁶ This pipeline flat-fields, wavelength-calibrates with respect to ThAr lamp spectra, extracts 1D spectra and subtracts the sky emission. We then used the *MINESweeper* code (Cargile et al. 2019) to forward-model the processed 1D spectra and infer stellar parameters, including radial velocities, $[\text{Fe}/\text{H}]$ and $[\alpha/\text{Fe}]$ abundances. For the analysis we retained 1160 well-fit spectra with $S/N \geq 3$. Radial velocities are measured to better than $\lesssim 1 \text{ km s}^{-1}$ (median $\sigma_v = 0.2 \text{ km s}^{-1}$), while typical uncertainties for $[\text{Fe}/\text{H}]$ and $[\alpha/\text{Fe}]$ are 0.06 dex and 0.04 dex, respectively. Despite the sub- km s^{-1} statistical

precision, sky-emission lines can show variations of up to $\approx 1 \text{ km s}^{-1}$ across the two camera chips and between different exposures. Our overall kinematic precision is therefore systematics-dominated at $\approx 1 \text{ km s}^{-1}$ ($\approx 0.2 \text{ pix}$), comparable to that typically achieved with Hectochelle (e.g., Caldwell et al. 2017).

3. Stream Membership

We define a sample of highly probable GD-1 member stars using their Gaia proper motions (Gaia Collaboration et al. 2018), de-reddened *Pan-STARRS* photometry (Schlegel et al. 1998; Chambers et al. 2016), and our measurements of radial velocity and metallicity. Figure 1 shows the adopted selection criteria in dashed pink, our spectroscopic sample in light blue, preliminary GD-1 members in medium blue, and final member selection in dark blue, with circles and stars for members in the main stream and the spur, respectively.

Following Price-Whelan & Bonaca (2018), we start with a generous selection in proper motions (corrected for solar reflex motion):

$$-10 < \mu_{\phi_1} < -5.5 \text{ mas yr}^{-1} \quad \text{and} \\ -2.5 < \mu_{\phi_2} < 2 \text{ mas yr}^{-1} \quad (\text{Figure 1, top-left panel}).$$

We further consider stars close to the $[\text{Fe}/\text{H}] = -2.3$, 12.6 Gyr isochrone at 8.5 kpc (Choi et al. 2016) as more likely GD-1 members (top-middle panel). The isochrone selection box is

⁶ <https://bitbucket.org/saotdc/hsred/>

tighter around the GD-1’s main sequence where the contrast with respect to the Milky Way field is higher, and wider along the red giant branch. Next, we require GD-1 members to have a small radial velocity offset from the GD-1’s orbit,⁷ $|\Delta V_r| < 7 \text{ km s}^{-1}$ (top-right panel). Finally, we select stars with $-2.37 < [\text{Fe}/\text{H}]_{\text{init}} < -1.75$ for a final sample of 43 most likely GD-1 stars (Figure 1, bottom panel). For membership selection we use the initial chemical composition, i.e., the composition of the gas the star was born with, to mitigate the effects of atomic diffusion, which operates in radiative zones of main-sequence stars and lowers their surface abundance of heavy elements (Dotter et al. 2017). In the interest of producing a pure sample, our spectroscopic selection criteria are rather stringent. Future analyses may improve the completeness of this sample using probabilistic membership approaches. The full spectroscopic sample with GD-1 membership flags we developed is publicly available.⁸

GD-1 stars in the main stream and in the spur have similar radial velocities and chemical abundances, demonstrating that the spur is indeed a part of GD-1. The stellar population in GD-1 is metal-poor, $[\text{Fe}/\text{H}] = -2.3 \pm 0.1$ (the initial iron abundance is lower, $[\text{Fe}/\text{H}]_{\text{init}} = -2.1 \pm 0.1$), and alpha-enhanced, $[\alpha/\text{Fe}] = 0.4 \pm 0.2$ (bottom panel of Figure 1). Abundance spreads in both $[\text{Fe}/\text{H}]$ and $[\alpha/\text{Fe}]$ can be accounted for by the measurement uncertainties, possibly indicating little intrinsic variation in chemical abundances, as commonly observed in globular clusters (Gratton et al. 2019). Combined with a low-velocity dispersion (Section 4), GD-1’s chemistry suggests the stream is a disrupted globular cluster.

4. GD-1 Kinematics

We summarize radial velocity structure of the GD-1 stream in Figure 2. The top panel shows the on-sky distribution of likely GD-1 members identified using Gaia proper motions (small points; Price-Whelan & Bonaca 2018), and highlights stars with a measured radial velocity (blue/orange for this work, gray for literature data from Koposov et al. 2010 and Huang et al. 2019). The second panel shows radial velocity as a function of the ϕ_1 stream coordinate. Our data include the first radial velocity measurements in the GD-1 spur (orange stars), and they are consistent with radial velocities in the main GD-1 stream (blue circles). Our measurements show a strong radial velocity gradient along the stream that is globally consistent with, but much more precisely determined compared to, the literature measurements obtained at a lower resolution. Our sample has five stars in common with Huang et al. (2019) and their radial velocities are consistent within the measurement uncertainty, indicating an absence of systematic biases in our catalog. We next search for orbits that fit the updated sample of GD-1 radial velocities.

We adopted the GD-1 orbit-fitting procedure from Price-Whelan & Bonaca (2018), including their fixed Milky Way model comprised of a $5.5 \times 10^{10} M_{\odot}$ Miyamoto & Nagai (1975) disk (scale height 28 pc, scale length 3 kpc), a $4 \times 10^9 M_{\odot}$ Hernquist (1990) bulge (scale radius 1 kpc), and a Navarro et al. (1997) halo (scale mass $7 \times 10^{11} M_{\odot}$, scale radius 15.62 kpc, z -axis flattening 0.95), as implemented in *gala* (Price-Whelan 2017). To constrain the GD-1 orbit, we used the compilation of 6D phase-space data from Price-

Whelan & Bonaca (2018) that we augmented with radial velocities from Huang et al. (2019) and this work. The radial velocity gradient of the best-fit orbit is shown with a black line in the second panel of Figure 2. The best-fit orbit has a pericenter at 13.8 kpc and an apocenter at 22.3 kpc, making the updated orbital solution slightly more circular, but otherwise similar to the orbit derived in Price-Whelan & Bonaca (2018).

In the third panel of Figure 2 we show the radial velocity offsets from the best-fit GD-1 orbit (black). Overall, our high-resolution measurements show little deviation from the orbital velocity and reveal a kinematically cold stream with a much lower dispersion than previously measured. Accounting for measurement uncertainties, the intrinsic velocity dispersion in GD-1 is $\lesssim 1 \text{ km s}^{-1}$. Repeat measurements of radial velocities with the same instrumental setup indicate that only slightly higher precision of 0.6 km s^{-1} can be achieved with MMT/Hectochelle (Cargile et al. 2019), so resolving the velocity dispersion in GD-1 may require higher-resolution spectroscopy.

To quantify the relative motion between the stream and the spur, we compare the median radial velocity of GD-1 members with respect to the best-fit orbit in individual Hectochelle fields (large symbols with a black outline, the errorbars are the standard deviation of relative radial velocities). At two locations where we observed the main stream and the spur in parallel ($\phi_1 = -33^{\circ}7, -30^{\circ}$), the relative radial velocity is smaller than 0.5 km s^{-1} , which is comparable to the measurement uncertainty. To a high degree, the GD-1 spur is comoving with the stream, which puts strong constraints on formation scenarios.

5. Discussion

We presented high-resolution spectroscopy at eight locations in the GD-1 stellar stream, distributed along the main stream and an adjacent spur. With the goal of discerning the association between the stream and the spur, we obtained the most precise radial velocities of GD-1 to date (statistical uncertainty $\lesssim 0.5 \text{ km s}^{-1}$). These data also update the GD-1’s orbit (Section 4), and will improve constraints on the Milky Way’s gravitational potential in future modeling of GD-1 (e.g., Koposov et al. 2010; Bowden et al. 2015). The relative radial velocity between the stream and the spur is small, $\Delta V_r \lesssim 1 \text{ km s}^{-1}$, which, combined with their similar metallicity, $[\text{Fe}/\text{H}] \approx -2.3$, suggests that the spur is a part of GD-1 that has been perturbed from an original orbit along the stream. We conclude with a discussion of implications that a comoving spur places on its formation mechanism and an outlook for dynamical inferences about the structure of the Milky Way if features like the GD-1 spur are common in other streams.

Bonaca et al. (2019b) showed that a stream can develop the spur-and-gap morphology similar to that observed in GD-1 following an encounter with a massive object. In this scenario, the spur can have a positive, negative, or no radial velocity offset with respect to the main stream, depending on the orbit of the perturber (Bonaca et al. 2019b, their models A, B, and C, respectively). Our data disfavor models with a negative radial velocity offset, like model B. On the other hand, models with a positive offset, like model A, seem consistent with the radial velocity gradient of the spur compared to the stream’s orbital radial velocity. However, there is little offset in radial velocities of the spur and main stream fields observed in parallel, similar to model C. Future modeling of GD-1’s entire radial velocity

⁷ We derived an updated GD-1 orbit in Section 4.

⁸ See https://github.com/abonaca/spur_rv.

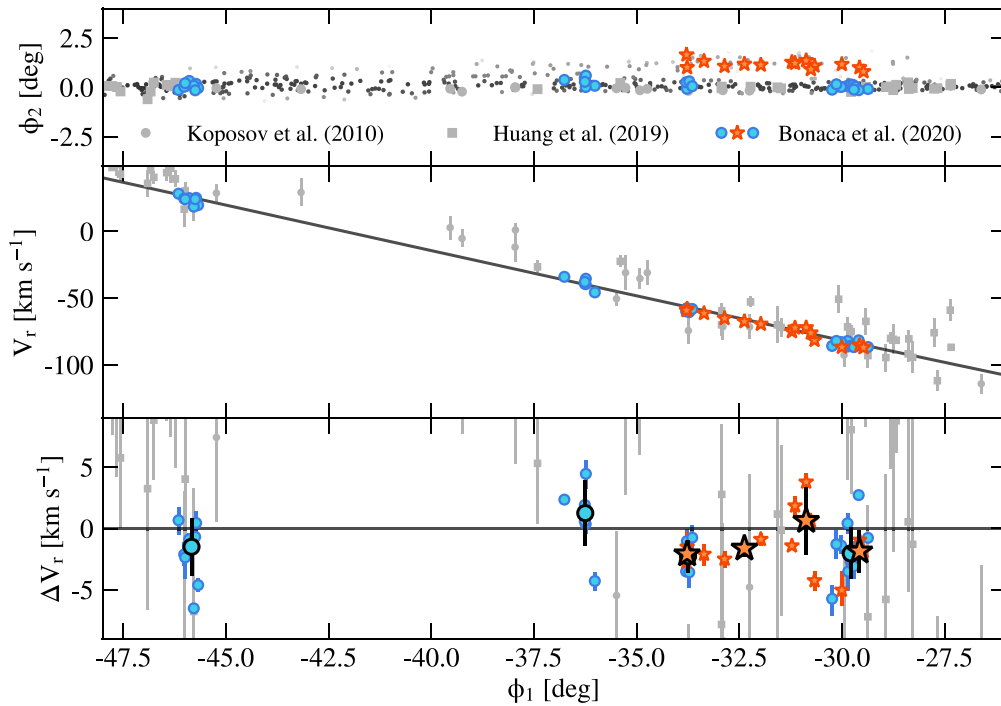


Figure 2. Sky positions of spectroscopically identified GD-1 members overplotted on the map of likely stream members (top; gray for literature data, blue circles and orange stars for the main stream and the spur data from this Letter, respectively). Both data sets agree that GD-1 has a steep radial velocity gradient (middle), which puts tight constraints on the stream’s orbit (black). At a fixed location along the stream, the median radial velocities of the main stream and the spur are consistent at a level of $\lesssim 1 \text{ km s}^{-1}$ (black-outlined symbols, bottom).

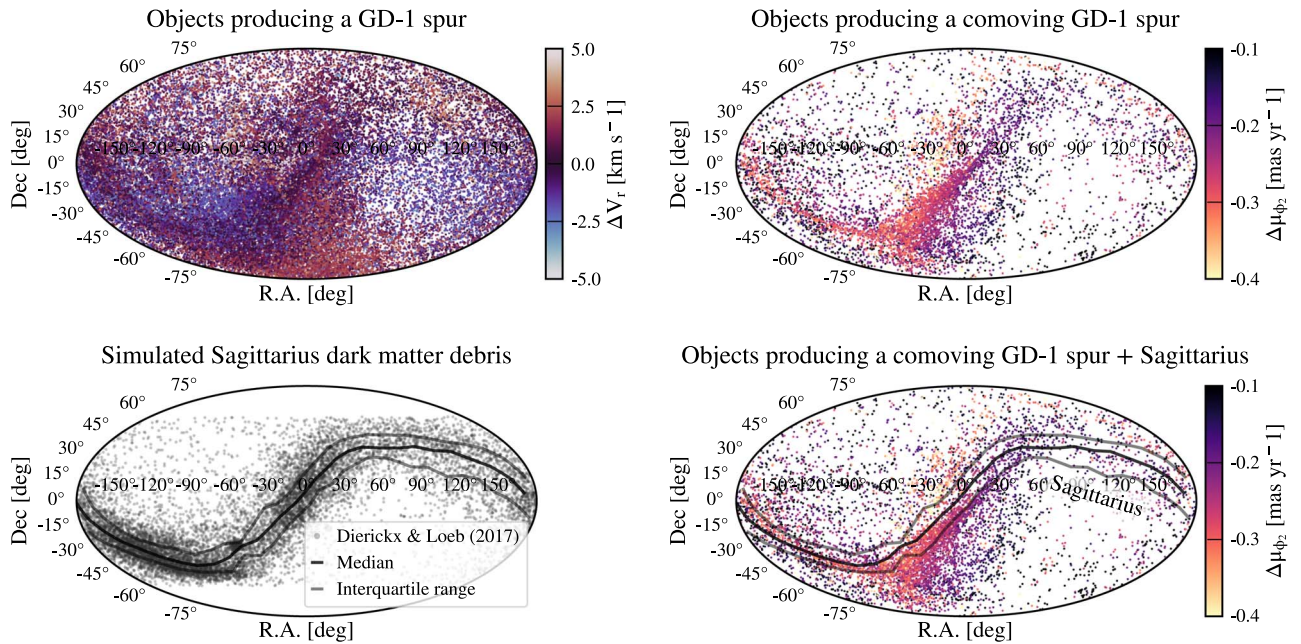


Figure 3. Present-day sky positions of objects sampled from a distribution that induces a spur-and-gap morphology after a close encounter with the GD-1 stream, color-coded by the relative radial velocity, ΔV_r , between the stream and the spur at $\phi_1 = -33^\circ.7$ (top left, from Bonaca et al. 2019b). Solutions that satisfy the measured radial velocity offset, $|\Delta V_r| < 1 \text{ km s}^{-1}$, are approximately on a great circle (top right), coincident with the distribution of dark matter expected from the disruption of the Sagittarius dwarf galaxy (bottom, gray points from Dierickx & Loeb 2017).

field will enable quantitative comparison of models with slight positive and no velocity offset. Here, we explore the broad implications of the observed GD-1 kinematics in the context of an encounter scenario by analyzing perturbed stream models from Bonaca et al. (2019b) with relative radial velocity $< 1 \text{ km s}^{-1}$ between the stream and the spur at the observed locations $\phi_1 = -33^\circ.7, -30^\circ$.

A spur comoving with the stream prefers models of a closer encounter (impact parameter $\lesssim 40 \text{ pc}$) with a less massive and more compact object (mass $5.4 \lesssim M/M_\odot \lesssim 7.3$, size $\lesssim 15 \text{ pc}$) than inferred from the stream morphology alone, while the range of allowed impact times between 0.1 and 1.5 Gyr ago, and the perturber’s total velocity ($\gtrsim 60 \text{ km s}^{-1}$) remain similar. The most substantial improvement that the kinematic data

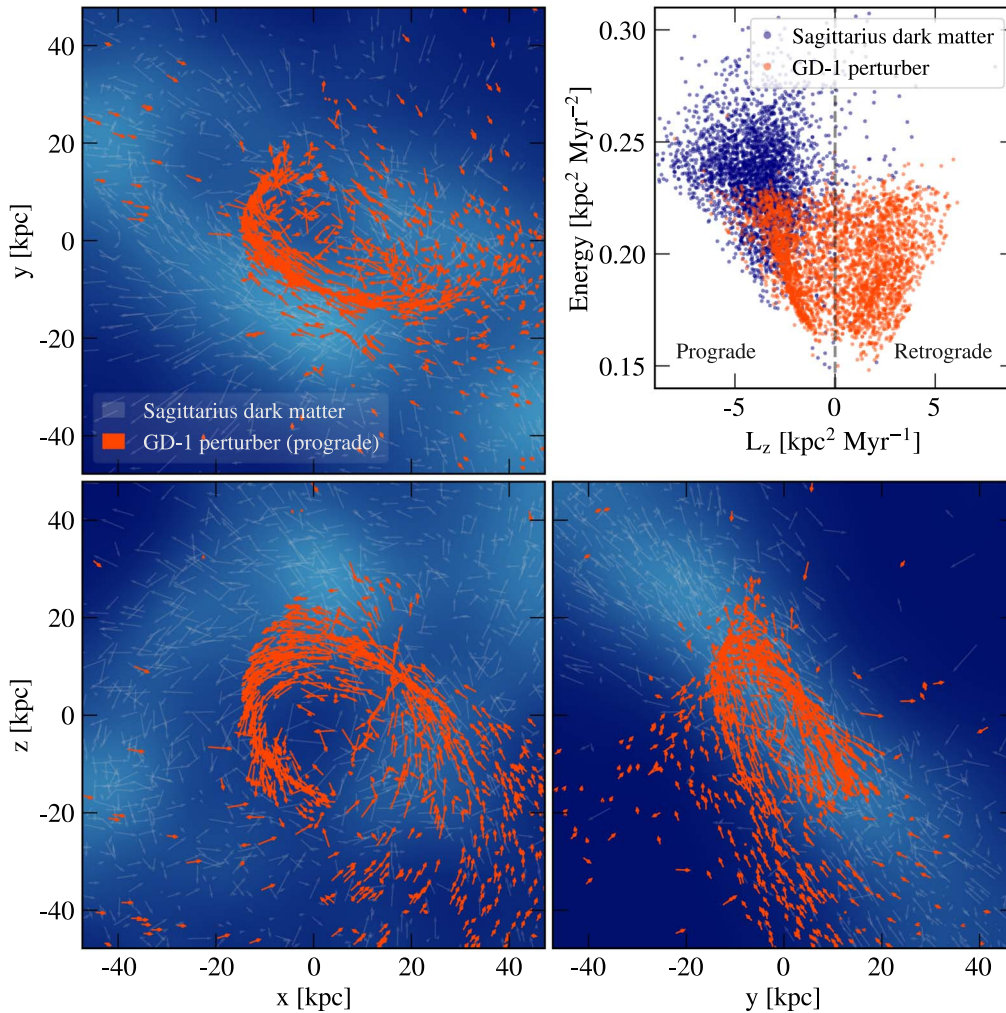


Figure 4. Phase-space distribution of plausible models for the GD-1 perturber (orange) matches the simulated distribution of dark-matter particles from the Sagittarius dwarf galaxy (blue). The largest overlap between the two populations is on low-energy prograde orbits (top-right panel). The remaining panels show that prograde models of the GD-1 perturber spatially and kinematically trace the Sagittarius stream of dark matter (lighter blue for higher Sagittarius density).

provide is in constraining the perturber’s orbit, which determines its present-day location. In the top left of Figure 3 we show the present-day sky positions of perturber models allowed by stream morphology, color-coded by the relative stream–spur radial velocity, $\Delta V_r(\phi_1 = -33^\circ)$. Morphology alone allows for a perturber on a variety of orbits, that result in present-day positions distributed across $\approx 30,000 \text{ deg}^2$. However, models satisfying a conservative estimate of the relative velocity, $|\Delta V_r| < 1 \text{ km s}^{-1}$, are spatially constrained to $\approx 5000 \text{ deg}^2$ (Figure 3, top right).

The relative radial velocity measured between the GD-1 stream and its spur improves the localization of the GD-1’s perturber by a factor of six, but the resulting area is still too wide for direct follow-up searches. Better localization is possible if we can measure the radial velocity gradient along the spur, generically expected in interaction models (Bonaca et al. 2019b). Radial velocities we measured in the GD-1 spur show a tentative gradient between $\phi_1 = -35^\circ$ and -31° (Figure 2, bottom), however, higher precision is required to fully resolve the gradient. Further improvements in the sky localization of the perturber are possible by measuring the relative proper motion between the GD-1 stream and the spur ($\Delta\mu_{\phi_2}$, color-coding in the right panels of Figure 3). At the present-day Gaia precision, the proper motion of the spur is

indistinguishable from the stream, $\Delta\mu_{\phi_2} = -0.2 \pm 0.9 \text{ mas yr}^{-1}$. We expect the more precise transverse velocities from Gaia (end-of-mission precision $\approx 0.25 \text{ mas yr}^{-1}$) or Hubble Space Telescope (3 yr baseline precision $\approx 0.1 \text{ mas yr}^{-1}$) will constrain the perturber’s location and enable direct follow-up.

Current localization of the GD-1 perturber suggests that it might originate from the Sagittarius dwarf galaxy. Dierickx & Loeb (2017) simulated disruption of Sagittarius that results in a distribution of dark-matter particles (Figure 3, bottom left) that overlap in projection with inferred positions of GD-1’s perturber (bottom right). To explore this scenario, we compare the full 6D phase-space of the GD-1 perturber and simulated dark matter from Sagittarius in Figure 4. The top-right panel shows the energy and z -component of the angular momentum for Sagittarius particles in blue and models of the GD-1 perturber in orange. Our data allow for a perturber on low-energy orbits with a wide range of angular momenta, which overlap the prograde orbits of Sagittarius at their low-energy end. The remaining panels of Figure 4 compare the velocity fields of Sagittarius dark-matter (blue arrows) and prograde models of the GD-1 perturber (orange arrows), overplotted on the smoothed Sagittarius density-field (counter-clockwise from the top left for the Galactocentric x - y , x - z , and y - z projections).

Viable GD-1 perturbers are distributed along the inner edge of the Sagittarius stream (light blue), and their velocity vectors are well aligned, further supporting possible association with Sagittarius. The possibility of GD-1's perturber originating from Sagittarius underlines the importance of accretion and time evolution in the Milky Way halo. Specifically, future tests of dark-matter substructure based on stream gaps will need to account for recently accreted subhalos in addition to the relaxed, isotropic population that has been assumed so far (e.g., Erkal et al. 2016; Banik et al. 2019).

A globular cluster or a dark-matter subhalo associated with Sagittarius are plausible culprits to produce the spur-and-gap morphology in GD-1, while the Sagittarius dwarf itself is too massive. Globular clusters appear more likely candidates due to the compact size we infer for the perturber, but none of the known clusters come closer than 1 kpc to the GD-1 impact site during the past 2 Gyr (based on the analysis from Bonaca et al. 2019b with the updated orbit of GD-1 and the 6D cluster positions from Baumgardt et al. 2019). Still, the scenario in which GD-1 was perturbed by a globular cluster needs to be further tested, as the census of globular clusters may be incomplete and the true gravitational potential likely deviates from the idealized model we used so far. If a luminous perturber is conclusively ruled out after these considerations have been taken into account, a dark-matter subhalo associated with Sagittarius remains a viable perturber, and its inferred high density might signal self-interacting dark matter (e.g., Kahlhoefer et al. 2019).

GD-1 is a stellar stream displaying many surprising features, which has sparked a discussion of additional processes to explain different aspects of the data. For example, de Boer et al. (2019) explored models in which GD-1 is perturbed by the Sagittarius dwarf galaxy. A strong interaction with Sagittarius can launch a long spur that remains closely aligned with GD-1 before detaching from the main stream (which reproduces the widening of GD-1 at $\phi_1 \lesssim -45^\circ$). On the other hand, Malhan et al. (2019a) discovered a low surface-brightness stream, Kshir, that intersects GD-1 at $\phi_1 \approx -20^\circ$. This cross-point is sufficiently close to the spur-and-gap feature that Kshir might have affected their formation. Alternatively, Webb & Bovy (2019) suggested that the gap at $\phi_1 \approx -40^\circ$ may not be a signature of an impact, but rather the location of the GD-1 progenitor's final disruption. In that case, the spur could be a result of substructure in the progenitor (e.g., Carlberg 2018), instead of forming through an external perturbation. Quantitative predictions for the spur kinematics formed in these processes are yet to be produced, but overall they are expected to impart large velocity kicks. Given our measurements of a comoving and kinematically cold spur, such processes may have had a limited role in GD-1's history.









We have shown that compact objects can be located in the Milky Way halo by dynamical modeling their impact on cold stellar streams like GD-1. The prospect of subhalo localization would revolutionize the study of dark matter in the Milky Way. Instead of inferring the nature of dark matter through the total abundance (e.g., Carlberg & Grillmair 2013) or the mass function of dark-matter subhalos (e.g., Banik et al. 2019), multi-wavelength observations of individual subhalo candidates would enable direct tests of different dark-matter models (e.g., Daylan et al. 2016), and add dark matter to the domain of multi-messenger astronomy.

It is a pleasure to thank Marion Dierickx for providing Sagittarius models, and Daniel Eisenstein, Doug Finkbeiner, Lars Hernquist, Sean Moran, and Hans-Walter Rix for valuable discussions. We also thank an anonymous referee for an extremely constructive report, and their insightful suggestions that have improved the scope and presentation of our work. Observations reported here were obtained at the MMT Observatory, a joint facility of the Smithsonian Institution and the University of Arizona. This project was developed in part at the 2019 Santa Barbara Gaia Sprint, hosted by the Kavli Institute for Theoretical Physics at the University of California, Santa Barbara. This research was supported in part at KITP by the Heising-Simons Foundation and the National Science Foundation under grant No. NSF PHY-1748958.

Facility: MMT(Hectochelle).

Software: *Astropy* (Astropy Collaboration et al. 2013; Price-Whelan et al. 2018), *gala* (Price-Whelan 2017), *IPython* (Pérez & Granger 2007), *matplotlib* (Hunter 2007), *numpy* (Walt et al. 2011), *scipy* (Jones et al. 2001).

ORCID iDs

Ana Bonaca  <https://orcid.org/0000-0002-7846-9787>
 Charlie Conroy  <https://orcid.org/0000-0002-1590-8551>
 David W. Hogg  <https://orcid.org/0000-0003-2866-9403>
 Phillip A. Cargile  <https://orcid.org/0000-0002-1617-8917>
 Nelson Caldwell  <https://orcid.org/0000-0003-2352-3202>
 Rohan P. Naidu  <https://orcid.org/0000-0003-3997-5705>
 Adrian M. Price-Whelan  <https://orcid.org/0000-0003-0872-7098>
 Joshua S. Speagle  <https://orcid.org/0000-0003-2573-9832>

References

- Astropy Collaboration, Robitaille, T. P., Tollerud, E. J., et al. 2013, *A&A*, **558**, A33
- Banik, N., Bovy, J., Bertone, G., Erkal, D., & de Boer, T. J. L. 2019, arXiv:1911.02662
- Baumgardt, H., Hilker, M., Sollima, A., & Bellini, A. 2019, *MNRAS*, **482**, 5138
- Bonaca, A., Conroy, C., Price-Whelan, A. M., & Hogg, D. W. 2019a, *ApJL*, **881**, L37
- Bonaca, A., Hogg, D. W., Price-Whelan, A. M., & Conroy, C. 2019b, *ApJ*, **880**, 38
- Bowden, A., Belokurov, V., & Evans, N. W. 2015, *MNRAS*, **449**, 1391
- Caldwell, N., Walker, M. G., Mateo, M., et al. 2017, *ApJ*, **839**, 20
- Cargile, P. A., Conroy, C., Johnson, B. D., et al. 2019, arXiv:1907.07690
- Carlberg, R. G. 2009, *ApJL*, **705**, L223
- Carlberg, R. G. 2018, *ApJ*, **861**, 69
- Carlberg, R. G., & Grillmair, C. J. 2013, *ApJ*, **768**, 171
- Carlberg, R. G., Grillmair, C. J., & Hetherington, N. 2012, *ApJ*, **760**, 75
- Chambers, K. C., Magnier, E. A., Metcalfe, N., et al. 2016, arXiv:1612.05560
- Choi, J., Dotter, A., Conroy, C., et al. 2016, *ApJ*, **823**, 102
- Daylan, T., Finkbeiner, D. P., Hooper, D., et al. 2016, *PDU*, **12**, 1
- de Boer, T. J. L., Erkal, D., & Gieles, M. 2019, arXiv:1911.05745
- Diemand, J., Kuhlen, M., Madau, P., et al. 2008, *Natur*, **454**, 735
- Dierickx, M. I. P., & Loeb, A. 2017, *ApJ*, **836**, 92
- D'Onghia, E., Springel, V., Hernquist, L., & Keres, D. 2010, *ApJ*, **709**, 1138
- Dotter, A., Conroy, C., Cargile, P., & Asplund, M. 2017, *ApJ*, **840**, 99
- Erkal, D., Belokurov, V., Bovy, J., & Sanders, J. L. 2016, *MNRAS*, **463**, 102
- Gaia Collaboration, Brown, A. G. A., Vallenari, A., et al. 2018, *A&A*, **616**, A1
- Gratton, R., Bragaglia, A., Carretta, E., et al. 2019, *A&ARv*, **27**, 8
- Grillmair, C. J., & Dionatos, O. 2006, *ApJL*, **643**, L17
- Hernquist, L. 1990, *ApJ*, **356**, 359
- Hopkins, P. F., Hernquist, L., Cox, T. J., Younger, J. D., & Besla, G. 2008, *ApJ*, **688**, 757
- Huang, Y., Chen, B. Q., Zhang, H. W., et al. 2019, *ApJ*, **877**, 13
- Hunter, J. D. 2007, *CSE*, **9**, 90
- Ibata, R. A., Lewis, G. F., Irwin, M. J., & Quinn, T. 2002, *MNRAS*, **332**, 915
- Ibata, R. A., Lewis, G. F., & Martin, N. F. 2016, *ApJ*, **819**, 1

- Johnston, K. V., Spergel, D. N., & Haydn, C. 2002, *ApJ*, 570, 656
- Jones, E., Oliphant, T., Peterson, P., et al. 2001, SciPy: Open Source Scientific Tools for Python, <http://www.scipy.org/>
- Kahlhoefer, F., Kaplinghat, M., Slatyer, T. R., & Wu, C.-L. 2019, *JCAP*, 2019, 010
- Koposov, S. E., Rix, H.-W., & Hogg, D. W. 2010, *ApJ*, 712, 260
- Malhan, K., Ibata, R. A., Carlberg, R. G., et al. 2019a, *ApJL*, 886, L7
- Malhan, K., Ibata, R. A., Carlberg, R. G., Valluri, M., & Freese, K. 2019b, *ApJ*, 881, 106
- Malhan, K., Ibata, R. A., & Martin, N. F. 2018, *MNRAS*, 481, 3442
- Meingast, S., Alves, J., & Fürnkranz, V. 2019, *A&A*, 622, L13
- Miyamoto, M., & Nagai, R. 1975, *PASJ*, 27, 533
- Navarro, J. F., Frenk, C. S., & White, S. D. M. 1997, *ApJ*, 490, 493
- Pérez, F., & Granger, B. E. 2007, *CSE*, 9, 21
- Price-Whelan, A. M. 2017, *JOSS*, 2, 388
- Price-Whelan, A. M., & Bonaca, A. 2018, *ApJL*, 863, L20
- Price-Whelan, A. M., Sipócz, B. M., Günther, H. M., et al. 2018, *AJ*, 156, 123
- Schlegel, D. J., Finkbeiner, D. P., & Davis, M. 1998, *ApJ*, 500, 525
- Shipp, N., Li, T. S., Pace, A. B., et al. 2019, *ApJ*, 885, 3
- Siegal-Gaskins, J. M., & Valluri, M. 2008, *ApJ*, 681, 40
- Springel, V., Wang, J., Vogelsberger, M., et al. 2008, *MNRAS*, 391, 1685
- Szentgyorgyi, A., Furesz, G., Cheimets, P., et al. 2011, *PASP*, 123, 1188
- Walt, S. v. d., Colbert, S. C., & Varoquaux, G. 2011, *CSE*, 13, 22
- Webb, J. J., & Bovy, J. 2019, *MNRAS*, 485, 5929
- Yoon, J. H., Johnston, K. V., & Hogg, D. W. 2011, *ApJ*, 731, 58